

# CALIS - a CALibration Insertion System for the DarkSide-50 dark matter search experiment

P. Agnes<sup>a</sup>, T. Alexander<sup>ae</sup>, A. Alton<sup>b</sup>, K. Arisaka<sup>ad</sup>, H.O. Back<sup>x</sup>,  
B. Balding<sup>g</sup>, K. Biery<sup>g</sup>, G. Bonfini<sup>q</sup>, M. Bossa<sup>i</sup>, A. Brigatti<sup>s</sup>, J. Brodsky<sup>x</sup>,  
F. Budano<sup>y</sup>, L. Cadonati<sup>ae</sup>, F. Calaprice<sup>x</sup>, N. Canci<sup>ad</sup>, A. Candela<sup>q</sup>,  
H. Cao<sup>x</sup>, M. Cariello<sup>h</sup>, P. Cavalcante<sup>q</sup>, A. Chavarria<sup>d</sup>, A. Chepurnov<sup>t</sup>,  
A.G. Cocco<sup>u</sup>, L. Crippa<sup>s</sup>, D. D'Angelo<sup>s</sup>, M. D'Incecco<sup>q</sup>, S. Davini<sup>k</sup>,  
M. De Deo<sup>q</sup>, A. Derbin<sup>v</sup>, A. Devoto<sup>c</sup>, F. Di Eusonio<sup>x</sup>, G. Di Pietro<sup>s</sup>,  
E. Edkins<sup>j</sup>, A. Empl<sup>k</sup>, A. Fan<sup>ad</sup>, G. Fiorillo<sup>u</sup>, K. Fomenko<sup>f</sup>, G. Forster<sup>ae</sup>,  
D. Franco<sup>a</sup>, F. Gabriele<sup>q</sup>, C. Galbiati<sup>x</sup>, A. Goretti<sup>x</sup>, L. Grandi<sup>d</sup>,  
M. Gromov<sup>t</sup>, M.Y. Guan<sup>l</sup>, Y. Guardincerri<sup>g</sup>, B. Hackett<sup>j</sup>, K. Herner<sup>g</sup>,  
E.V. Hungerford<sup>k</sup>, Al. Ianni<sup>q</sup>, An. Ianni<sup>x</sup>, C. Jollet<sup>aa</sup>, K. Keeter<sup>e</sup>,  
C. Kendziora<sup>g</sup>, S. Kidner<sup>af,1</sup>, V. Kobylev<sup>n</sup>, G. Koh<sup>x</sup>, D. Korblev<sup>f</sup>,  
G. Korga<sup>k</sup>, A. Kurlej<sup>ae</sup>, P.X. Li<sup>l</sup>, B. Loer<sup>x</sup>, P. Lombardi<sup>s</sup>, C. Love<sup>ab</sup>,  
L. Ludhova<sup>s</sup>, S. Luitz<sup>z</sup>, Y.Q. Ma<sup>l</sup>, I. Machulin<sup>o,r</sup>, A. Mandarano<sup>i</sup>, S. Mari<sup>y</sup>,  
J. Maricic<sup>j</sup>, L. Marini<sup>y</sup>, C.J. Martoff<sup>ab</sup>, A. Meregaglia<sup>aa</sup>, E. Meroni<sup>s</sup>,  
P.D. Meyers<sup>x</sup>, R. Milincic<sup>j</sup>, D. Montanari<sup>g</sup>, A. Monte<sup>ae</sup>, M. Montuschi<sup>q</sup>,  
M.E. Monzani<sup>z</sup>, P. Mosteiro<sup>x</sup>, B. Mount<sup>e</sup>, V. Muratova<sup>v</sup>, P. Musico<sup>h</sup>,  
A. Nelson<sup>x</sup>, S. Odrowski<sup>q</sup>, M. Okounkova<sup>x</sup>, M. Orsini<sup>q</sup>, F. Ortica<sup>w</sup>,  
L. Pagani<sup>h</sup>, M. Pallavicini<sup>h</sup>, E. Pantic<sup>ad,ac</sup>, L. Papp<sup>af</sup>, S. Parmeggiano<sup>s</sup>,  
R. Parsells<sup>x</sup>, K. Pelczar<sup>m</sup>, N. Pelliccia<sup>w</sup>, S. Perasso<sup>a</sup>, A. Pocar<sup>ae</sup>,  
S. Pordes<sup>g</sup>, D. Pugachev<sup>o</sup>, H. Qian<sup>x</sup>, K. Randle<sup>ae</sup>, G. Ranucci<sup>s</sup>,  
A. Razeto<sup>q</sup>, B. Reinhold<sup>j,\*</sup>, A. Renshaw<sup>ad</sup>, A. Romani<sup>w</sup>, B. Rossi<sup>x,u</sup>,  
N. Rossi<sup>q</sup>, S.D. Rountree<sup>af</sup>, D. Sablone<sup>k</sup>, P. Saggese<sup>q</sup>, R. Saldanha<sup>d</sup>,  
W. Sands<sup>x</sup>, S. Sangiorgio<sup>p</sup>, E. Segreto<sup>q</sup>, D. Semenov<sup>v</sup>, E. Shields<sup>x</sup>,  
M. Skorokhvatov<sup>o,r</sup>, O. Smirnov<sup>f</sup>, A. Sotnikov<sup>f</sup>, C. Stanford<sup>x</sup>,  
Y. Suvorov<sup>ad</sup>, R. Tartaglia<sup>q</sup>, J. Tatarowicz<sup>ab</sup>, G. Testera<sup>h</sup>, A. Tonazzo<sup>a</sup>,  
E. Unzhakov<sup>v</sup>, R.B. Vogelaar<sup>af</sup>, M. Wada<sup>x</sup>, S. Walker<sup>u</sup>, H. Wang<sup>ad</sup>,  
Y. Wang<sup>l</sup>, A. Watson<sup>ab</sup>, S. Westerdale<sup>x</sup>, M. Wojcik<sup>m</sup>, A. Wright<sup>x</sup>,  
X. Xiang<sup>x</sup>, J. Xu<sup>x</sup>, C.G. Yang<sup>l</sup>, J. Yoo<sup>g</sup>, S. Zavatarelli<sup>h</sup>, A. Zec<sup>ae</sup>, C. Zhu<sup>x</sup>,  
G. Zuzel<sup>lm</sup>

---

\*Corresponding authors:

Email address: bernd@hawaii.edu (B. Reinhold)

<sup>1</sup>Deceased

- <sup>a</sup>APC, Université Paris Diderot, Sorbonne Paris Cité, Paris 75205, France  
<sup>b</sup>Physics and Astronomy Department, Augustana College, Sioux Falls, SD 57197, USA  
<sup>c</sup>Physics Department, Università degli Studi and INFN, Cagliari 09042, Italy  
<sup>d</sup>Kavli Institute, Enrico Fermi Institute and Dept. of Physics, University of Chicago, Chicago, IL 60637, USA  
<sup>e</sup>School of Natural Sciences, Black Hills State University, Spearfish, SD 57799, USA  
<sup>f</sup>Joint Institute for Nuclear Research, Dubna 141980, Russia  
<sup>g</sup>Fermi National Accelerator Laboratory, Batavia, IL 60510, USA  
<sup>h</sup>Physics Department, Università degli Studi and INFN, Genova 16146, Italy  
<sup>i</sup>Gran Sasso Science Institute, L’Aquila 67100, Italy  
<sup>j</sup>Department of Physics and Astronomy, University of Hawai’i, Honolulu, HI 96822, USA  
<sup>k</sup>Department of Physics, University of Houston, Houston, TX 77204, USA  
<sup>l</sup>Institute of High Energy Physics, Beijing 100049, China  
<sup>m</sup>Smoluchowski Institute of Physics, Jagiellonian University, Krakow 30059, Poland  
<sup>n</sup>Institute for Nuclear Research, National Academy of Sciences of Ukraine, Kiev 03680, Ukraine  
<sup>o</sup>National Research Centre Kurchatov Institute, Moscow 123182, Russia  
<sup>p</sup>Lawrence Livermore National Laboratory, 7000 East Avenue, Livermore, CA 94550  
<sup>q</sup>Laboratori Nazionali del Gran Sasso, Assergi (AQ) 67010, Italy  
<sup>r</sup>National Research Nuclear University MEPhI (Moscow Engineering Physics Institute), 115409 Moscow, Russia  
<sup>s</sup>Physics Department, Università degli Studi and INFN, Milano 20133, Italy  
<sup>t</sup>Skobeltsyn Institute of Nuclear Physics, Lomonosov Moscow State University, Moscow 119991, Russia  
<sup>u</sup>Physics Department, Università degli Studi Federico II and INFN, Napoli 80126, Italy  
<sup>v</sup>St. Petersburg Nuclear Physics Institute, Gatchina 188350, Russia  
<sup>w</sup>Chemistry, Biology and Biotechnology Department, Università degli Studi and INFN, Perugia 06123, Italy  
<sup>x</sup>Department of Physics, Princeton University, Princeton, NJ 08544, USA  
<sup>y</sup>Physics Department, Università degli Studi Roma Tre and INFN, Roma 00146, Italy  
<sup>z</sup>SLAC National Accelerator Laboratory, Menlo Park, CA 94025, USA  
<sup>aa</sup>IPHC, Université de Strasbourg, CNRS/IN2P3, Strasbourg 67037, France  
<sup>ab</sup>Physics Department, Temple University, Philadelphia, PA 19122, USA  
<sup>ac</sup>Physics Department, University of California, Davis, CA 95616, USA  
<sup>ad</sup>Physics and Astronomy Department, University of California, Los Angeles, CA 90095, USA  
<sup>ae</sup>Amherst Center for Fundamental Interactions and Physics Department, University of Massachusetts, Amherst, MA 01003, USA  
<sup>af</sup>Physics Department, Virginia Tech, Blacksburg, VA 24061, USA

---

## Abstract

This report describes design, fabrication, commissioning and use of a calibration source insertion system (CALIS) in DarkSide-50 experiment.

CALIS deploys radioactive sources into liquid scintillator veto to characterize detector response and detection efficiency of DarkSide-50 Liquid Argon Time Projection Chamber used for dark matter detection, and surrounding 30 t organic liquid scintillator neutron veto. It was commissioned in September 2014 and used successfully in several campaigns to deploy gamma and neutron sources since then. A description of hardware and highlights from calibration analysis results are given below.

*Keywords:*

Dark matter, WIMP, Noble liquid detectors, Low-background detectors, Liquid scintillators, radioactive source calibration

PACS: 95.35.+d, 29.40.Mc, 29.40Gx

---

## **1 Contents**

<b>2 1 Introduction</b>	<b>4</b>
<b>3 2 Design Requirements &amp; Hardware Implementation</b>	<b>4</b>
2.1 Purpose . . . . .	4
2.2 Deployment & Articulation Mechanism . . . . .	6
2.3 CALIS Enclosure & Scintillator . . . . .	10
2.4 Deployment Device . . . . .	11
2.5 Source Holder and Arms . . . . .	12
2.6 Hardware Details and Safety Features . . . . .	12
2.7 System's degrees of freedom . . . . .	14
<b>11 3 Testing, Cleaning and Commissioning</b>	<b>16</b>
<b>12 4 Calibration Campaigns</b>	<b>17</b>
4.1 Radioactive Sources . . . . .	17
4.2 Calibration Campaigns Timeline and Stability . . . . .	17
4.3 TPC Calibration . . . . .	19
4.4 Liquid Scintillator Veto . . . . .	21
<b>17 5 Conclusions</b>	<b>23</b>
<b>18 6 Acknowledgements</b>	<b>23</b>

*keywords  
and PACS  
are from our  
papers - need  
updates?*

## 19 1. Introduction

20 DarkSide-50 is a Liquid Argon Time Projection Chamber (LAr TPC),  
21 operated in Italy's Gran Sasso National Laboratory (LNGS) to search for  
22 nuclear recoils induced by weakly interacting massive particles (WIMPs).  
23 The first physics result was reported in [1] based on 50 live data collection  
24 days with Atmospheric Argon (AAr), providing the most sensitive limit  
25 on a dark matter search using a LAr TPC to date with a 90% CL upper  
26 limit on the WIMP-nucleon spin-independent cross section of  $6.1 \times 10^{-44}$   
27  $\text{cm}^2$  for a WIMP mass of 100 GeV/c<sup>2</sup>.

28 A first WIMP search using argon extracted from underground sources  
29 (Underground Argon, UAr) has been reported in [2], following the WIMP  
30 search with AAr. UAr has a lower concentration of the radioactive  $\beta$ -  
31 emitter  $^{39}\text{Ar}$  by a factor  $(1.4 \pm 0.2) \times 10^3$  relative to AAr. Calibration  
32 campaigns have been performed in the presence of AAr and UAr.

33 DarkSide-50 apparatus is described in detail in [1]. As shown in fig. 1  
34 it features a LAr TPC surrounded by a 30 t liquid scintillator-based veto  
35 (LSV) system, placed inside a water Cerenkov veto detector (WCV), both  
36 which measure in-situ and suppress radiogenic and cosmogenic back-  
37 grounds. On WCV's top is a radon-free clean room (CRH) housing the  
38 cryogenic supply system and electronics (Fig. 2). The LSV's inside is ac-  
39 cessible from CRH through four access ports called organ pipes closed by  
40 gate valves.

### 41 *Laser calibration*

42 WCV, LSV and TPC electronics gain calibration is performed with  
43 dedicated Laser systems, in place in each of three subdetectors. WCV  
44 laser calibration is sufficient to veto muons (and their secondaries) with  
45 high efficiency. TPC detector response has been calibrated using the inter-  
46 nal  $^{39}\text{Ar}$  and  $^{83m}\text{Kr}$ , that has been added into LAr recirculation system  
47 during dedicated calibration campaigns [1].

## 48 2. Design Requirements & Hardware Implementation

### 49 2.1. Purpose

50 CALibration Insertion System (CALIS) deploys radioactive gamma  
51 and neutron sources inside the LSV to study and calibrate TPC and LSV  
52 detector response and neutron detection efficiency. This complements

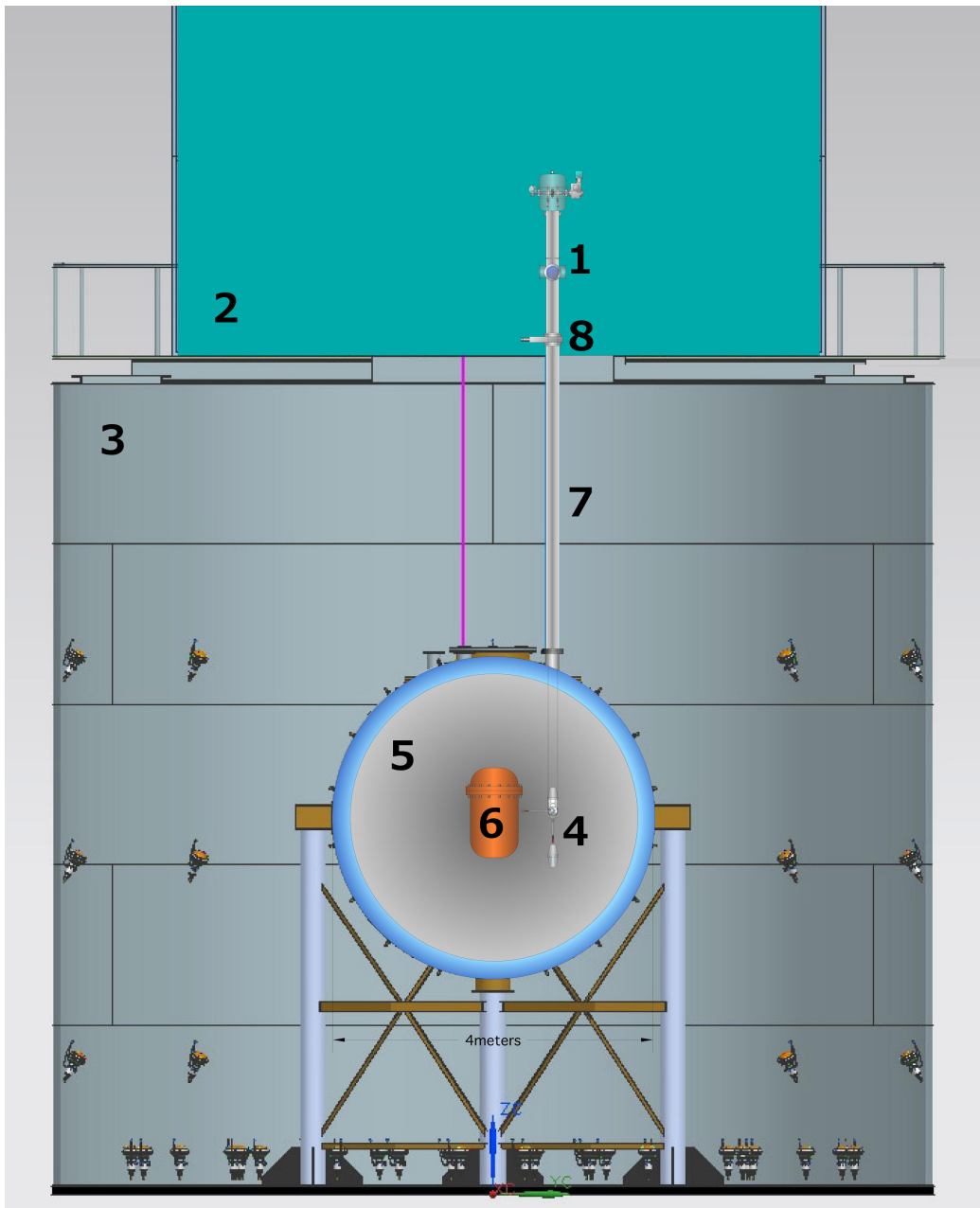


Figure 1: A conceptual drawing of CALIS (1) installed in radon-free clean room CRH (2) atop water Cerenkov veto (WCV, 3) and with deployment device (4) containing the source deployed in liquid scintillator veto (LSV, 5) next to liquid argon time projection chamber's (LAr TPC) cryostat (6). Clean room and LSV are connected through four access ports called organ pipes (only one of which is drawn in above sketch: (7)). All four organ pipes end in CRH at gate valves (8) which can be manually opened or closed. During normal operations all four organ pipes are closed. Not included in sketch are tubes connecting cryogenic systems in CRH to cryostat in LSV [3].

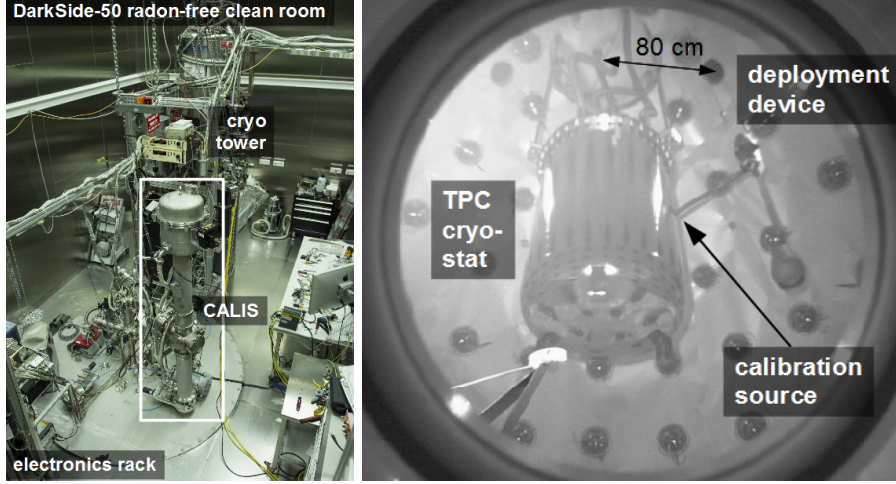


Figure 2: *left*: CALIS after installation inside radon-free clean room CRH. The organ pipe is 80 cm off-center with respect to TPC’s vertical Z-axis. *right*: Photograph taken with a camera looking upwards into LSV from the bottom. It shows source deployment device deployed through one of the organ pipes visible on top right. The arm is articulated and source is next to LAr TPC’s cryostat [3].

53 and extends internal calibration sources’ and laser calibration’s physics  
54 reach.

55 LSV’s center is about 6 m below gate valve inside CRH and 15 cm  
56 diameter wide organ pipes are 80 cm off TPC’s vertical Z-axis as shown in  
57 Fig. 2. For TPC calibration the radioactive source has to be positioned in  
58 immediate contact with cryostat, in order to minimize rate losses through  
59 absorption in particular for low energy sources such as  $^{57}\text{Co}$  (122 keV).

## 60 2.2. Deployment & Articulation Mechanism

61 This requirement precludes a single cable solution deployed from  
62 within a glove box used in several scintillator experiments [4, 5]. As  
63 shown in Figs. 2 and 3 this apparatus consists instead of an enclosure,  
64 which has been installed in CRH and the deployment device is attached  
65 to enclosure through two stainless steel cables wound up on cable spools  
66 and allow lowering of device into LSV, next to cryostat.

67 A stepper motor moves both cable spools concurrently and sends de-  
68 ployment device into LSV. An absolute encoder provides its current po-  
69 sition, even in absence of power. The stepper motor is controlled via a  
70 simple graphical LabVIEW interface, run on a dedicated laptop, in which  
71 current Z-position is shown and a target Z-position can be provided by

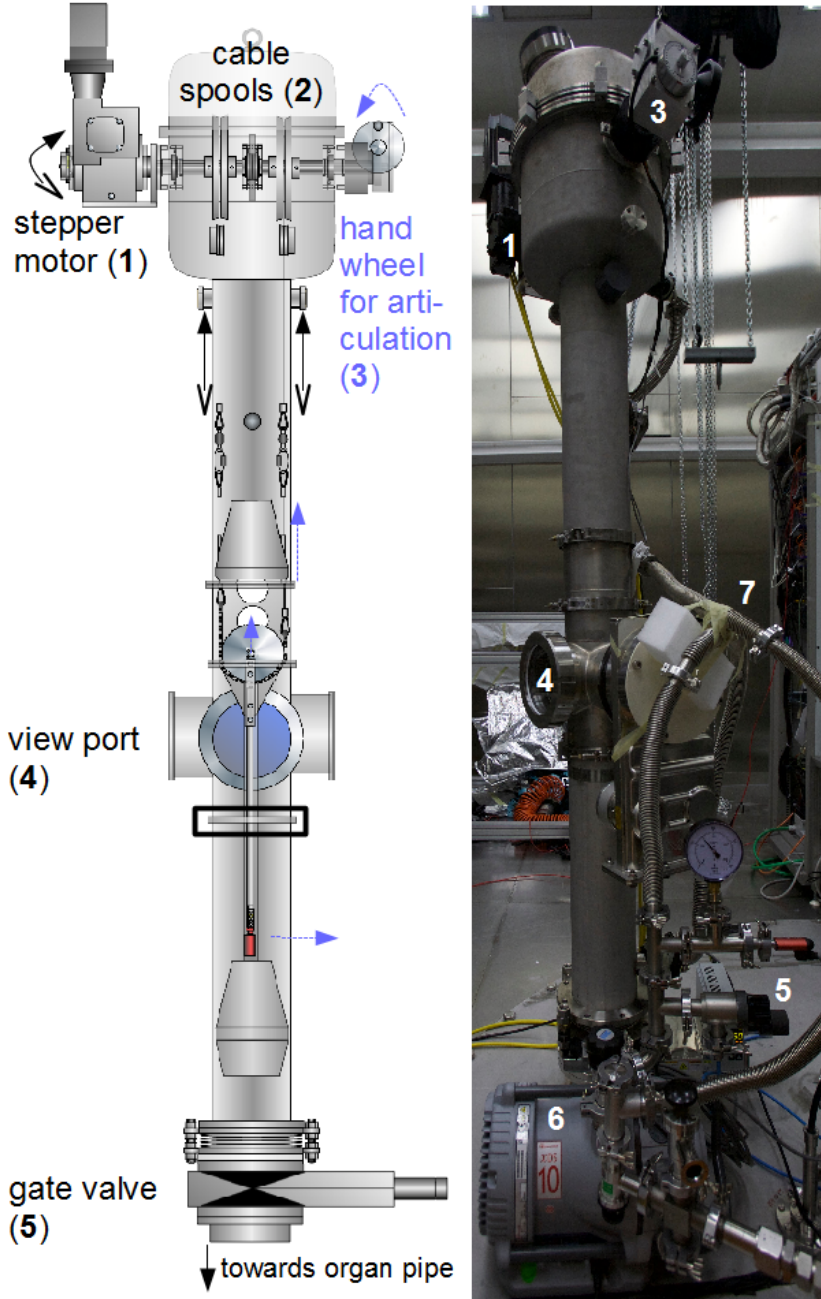


Figure 3: Mechanical drawing of CALIS showing the housing and the deployment device in its home position. The total height is approx. 240 cm including the gate valve.) The two modes of operation are illustrated: In order to move the deployment device down into the LSV or back up the stepper motor moves both cable spools (2) simultaneously. In order to articulate, the articulation wheel (3) is rotated manually, which affects only the right spool, thereby shortening the right cable with respect to the left cable thereby articulating the arm and lifting the pivot center. The amount of lifting and the amount of rotations until a horizontal articulation is reached has been calibrated prior to installation in CRH (Sec. 3). In the photograph the vacuum pump (6) and tubing (7) are shown, which are part of the evacuation and purging system (Sec. 2.3).

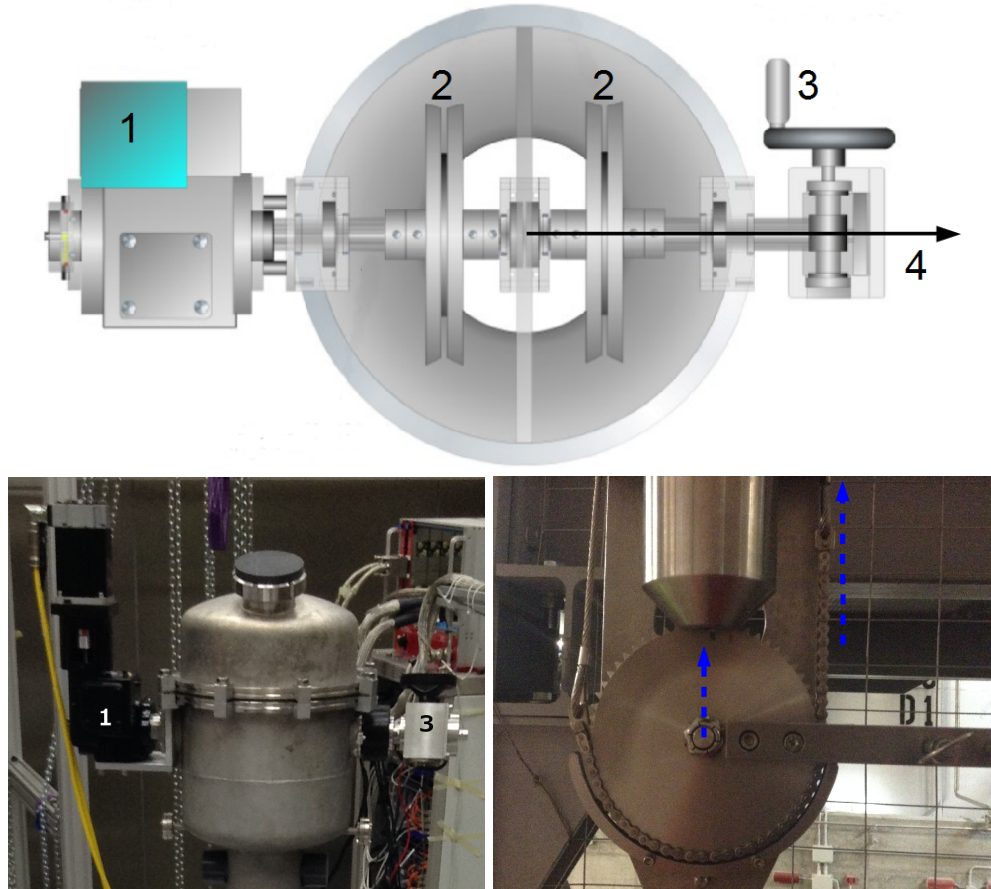


Figure 4: *top*: Inside view of drive mechanism's components seen from top of CALIS. Stepper motor inside motor housing (1) drives both cable spools (2) concurrently, thereby lowering calibration device into LSV. An absolute encoder provides deployment device's current position. Hand wheel (3) turns right spool only, thereby transferring the rotation of articulation wheel into a (de)articulation of the source arm (*bottom right*). Arrow (4) in the sketch points in same direction as horizontally articulated arm. Chain has a guard rail, ensuring chain can never come off the gear.

72 the operator. Z-positions are given in motor step counts, an arbitrary unit  
 73 which has been calibrated outside CRH in meters (Fig. 5) and relative to  
 74 TPC using calibration data's t-drift distributions (Fig. 12).

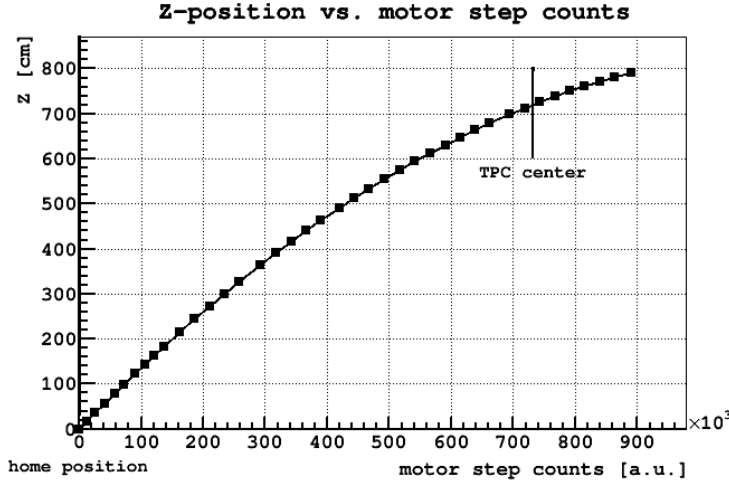


Figure 5: Deployment device's Z-position versus motor's step counts. Non-linear correspondence between number of steps and cable length deployed arises as follows: As cable winds around spool, the winding radius changes, increasing as deployment device is lifted and decreasing as it is lowered. A motor step count corresponds to a fixed angular distance  $d\theta$ , yet amount of cable deployed during this motor step count is *winding radius*  $\cdot d\theta$ . As winding radius changes as a function of Z-position, fraction of deployed cable per motor step count changes. Home position is at 0, the TPC center is reached after more than 7m of travel into the LSV.

75 Arm articulation is done manually via articulation wheel. This affects  
 76 only cable spool close to articulation wheel, the left one in Fig. 4, thereby  
 77 shortening right cable with respect to the left cable and engaging gear  
 78 through a chain (Fig. 4). As a result arm is articulated and pivot cen-  
 79 ter is lifted. Non-linearity arising from the change in winding radius on  
 80 cable spools affects also amount of rotation required by hand wheel for  
 81 horizontal source arm articulation. Degrees on the articulation wheel cor-  
 82 responding to a horizontal articulation have been calibrated as a function  
 83 of cable length deployed prior to installation in CRH.

84 Articulation and a movement in z-direction are mutually exclusive  
 85 since arm articulation leads to more wound up cable on spool close to  
 86 articulation wheel with respect to the other. If then in deployment mode

87 both spools would be rotated simultaneously with same angular speed,  
88 cable close to articulation wheel would wind up faster than the other,  
89 leading to a build up of difference in cable length and the deployment  
90 device would only be hanging on one cable. In order to avoid an imbal-  
91 anced z-movement arm has to be dearticulated fully before a change in z-  
92 position can be initiated. This is enforced by an electric switch preventing  
93 z-movement, which is disengaged only when arm is fully dearticulated  
94 (vertical).

### 95 2.3. CALIS Enclosure & Scintillator

96 Besides providing mechanical support for deployment device via ca-  
97 ble spools, the CALIS enclosure is an important interface between radon-  
98 free clean room CRH and LSV, through which sources are exchanged.  
99 The enclosure protects liquid scintillator (LS) and eliminates human con-  
100 tact with any traces of harmful LS vapor (Fig. 3). It plays same role as a  
101 glove box for similar calibration systems yet with a narrower foot print  
102 inside CRH. Liquid scintillator is a mixture of PC and TMB<sup>2</sup> with the  
103 wavelength shifter PPO [3]. It may not get exposed to oxygen or water as  
104 is present in normal clean room air. Contamination of LS with  $^{222}\text{Rn}$  and  
105 its long-lived radioactive daughters has to be avoided, too.

106 Going up from gate valve on which CALIS has been installed, there is  
107 a teflon disk that can electrically isolate CALIS from ground, even though  
108 during normal operations CALIS housing is connected to ground. A tri-  
109 pod with a bellow has been used to vertically align enclosure right after  
110 installation on gate valve. Bellow is connected to a 59.4 cm long cylindri-  
111 cal stainless steel enclosure pipe. It has same diameter as an organ pipe  
112 (15 cm) and connects to the view port above by a ring clamp, which plays  
113 a critical role in XY-rotations (see Sec. 2.7.1). View port can be opened  
114 for handling source arm and exchanging sources. Everything above ring  
115 clamp forms upper assembly. It features a stainless steel cylindrical en-  
116 closure housing cable drive mechanism, including cable spools, stepper  
117 motor and articulation mechanism already described in Sec. 2.2.

### 118 Vacuum evacuation (flushing) and nitrogen purging system

119 One of this system's most important safety features is making sure  
120 that TMB and PC residue on device are extracted from CALIS prior to

---

<sup>2</sup>The concentration of TMB has varied during campaigns (see Sec. 4).

121 opening access ports to exchange source or arms. This is important for  
122 safe working conditions inside CRH as well as for the scintillator and  
123 radiopurity.

124 After source arm insertion and view port closure inside of CALIS  
125 housing is filled with normal air, that is damaging to the scintillator.  
126 A sequence of evacuations and nitrogen purges reduces fraction of air  
127 including its contaminants (water vapor, oxygen, radioactivity) to negligi-  
128 gible levels. Only after this sequence is finalized gate valve is opened and  
129 deployment device is introduced into LSV. Evacuation is achieved with a  
130 vacuum pump and exhaust air is removed through dedicated vent lines  
131 (Fig. 3).

132 At calibration campaign's end, after deployment device has returned  
133 to its home position inside enclosure and gate valve has been closed, scin-  
134 tillator vapor, and in particular TMB, has to be removed prior to opening  
135 view port. Again an evacuation and nitrogen purges sequence is em-  
136 ployed. By lowering pressure inside of CALIS below TMB and PC vapor  
137 pressure, scintillator evaporates and gets removed through vacuum pump  
138 vent line. Once pressure inside housing stays consistently below vapor  
139 pressure of TMB all scintillator has been removed and view port can be  
140 opened to access source arm.

#### 141 *Material Compatibility*

142 All materials coming in contact with scintillator veto are made of stain-  
143 less steel and teflon except for sealing o-rings which are made of viton.  
144 All three materials are certified materials for contact with all scintillator  
145 components including TMB and PC.

#### 146 *2.4. Deployment Device*

147 Deployment device (Fig. 3) contains arm support structure which  
148 holds source at its end. Device is equipped with tapered cones on its  
149 top and bottom ensuring that ends do not get snagged on organ pipe's  
150 inner edges as it moves down and up. It is attached to housing by two  
151 cables. Swivel hooks are employed in cables' attachment to deployment  
152 device allowing cables to move freely and not get tangled. There are two  
153 weights built into the device, one cylindrical in conical cap above rota-  
154 tion gear mechanism and one inside cones at device's bottom end. Both  
155 help to minimize any lateral motion or oscillations during deployment,  
156 articulation and dearticulation especially. It also ensures smooth motion

157 of deployment device into organ pipe and back to home position inside  
158 CALIS housing.

159 *2.5. Source Holder and Arms*

160 A source arm and source holder are attached to an articulation gear  
161 (Fig. 6). Different arm lengths have been prepared with a maximum 62  
162 cm arm length, arm length thereby being measured from pivot point of  
163 rotation gear to source holder's tip. This arm length allows source to be  
164 placed in immediate contact with cryostat (Fig. 2, right), as organ pipe's  
165 center axis is 80 cm from TPC center and cryostat has an outer radius of  
166 32 cm. The 62 cm arm was used for deployments in past calibration cam-  
167 paigns (Sec. 4). Inside source holder radioactive source is placed, pressed  
168 to tip and held in place via a spring during deployment, articulation and  
169 dearticulation. Source holder is sealed such that no liquid scintillator can  
170 enter during deployment. This has also been verified during each source  
171 extraction and no liquid traces have been found on its inside.

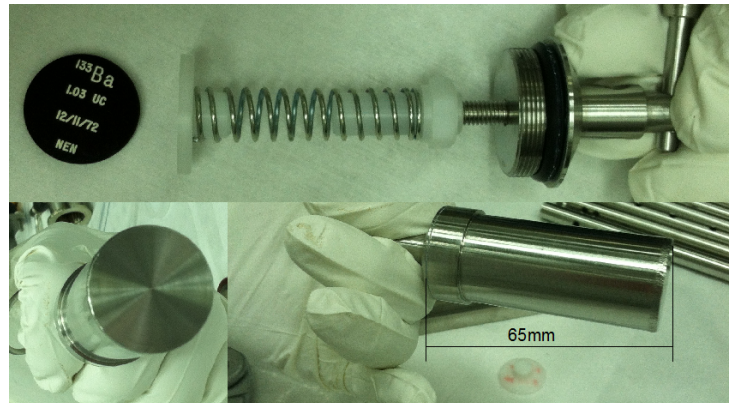


Figure 6: Source holder that connects to an arm and to the articulation gear of the deployment device. The source, here a  $^{133}\text{Ba}$  source, is pressed to the tip of the source holder via a spring.

172 *2.6. Hardware Details and Safety Features*

173 CALIS offers various safety features ensuring that this device runs  
174 smoothly, no components are lost inside detector, avoid any detector  
175 contamination by dirty or incompatible materials, maintain pressure and  
176 avoiding introducing oxygen or water in contact with LS and TMB.

177 **Cable strength:** Deployment device holding cables are rated for loads  
178 over 1300 lbs, while deployment device weight is at the level of 20-  
179 30 lbs, thus well below cable's breaking strength.

180 **Drive mechanism:** If a power failure occurs, the magnetic break ensures  
181 deployment device does not move. Servo motor torque is limited  
182 in case of an unexpected load and the risk of breaking the cable is  
183 avoided.

184 Speed reducer (gears) is a double worm gear design. Primary worm  
185 gear has a 50:1 reduction and secondary worm has a 82:1 reduc-  
186 tion. Servo motor input speed is 2400 RPMs, output is 0.6 RPM and  
187 weight capacity is 148 lbs. If a power failure occurs speed reducer  
188 can hold load at any position without back drive. Motor speed has  
189 been limited to 0.4 cm/s minimizing any lateral oscillation of de-  
190 ployment device during lowering and raising the source. This is  
191 maximum speed at which motor does not overheat.

192 **Manual retraction system:** It is possible to manually retract deployment  
193 device back to its home position and close gate valve in unlikely  
194 case of complete motor failure while source is deployed. Motor is  
195 disengaged, and a wrench is used to manually wind cable back on  
196 spools and retract deployment device back above gate valve.

197 **High limit switch:** A high limit switch is a hardware interlock, that pre-  
198 vents deployment device hitting cable spools and gears, should it  
199 pass beyond home position in CALIS housing (Fig. 3).

200 *Neither manual retraction system had to be used so far nor has high limit*  
201 *switch been activated during calibration campaigns.*

202 **Light and leak tightness of CALIS:** When deployment device is next to  
203 cryostat gate valve is open and data is also taken with LSV. A re-  
204 quirement is an absolute light tight and pressure leak tight housing.  
205 All view ports are covered with light tight covers when organ pipe  
206 gate valve is open. Both light and leak tightness was extensively  
207 validated throughout manufacturing process, commissioning and  
208 during calibration campaigns (Sec. 3).

209 **Securing source:** All connection points for source and arm have been se-  
210 cured with two push locking pins that cannot be disengaged with-

211 out a person pressing the pin. In addition, source holder and two  
 212 locking pins are all tethered from outside view port until they are  
 213 locked in place eliminating possibility of accidentally falling into  
 214 CALIS housing's interior.

215 *2.7. System's degrees of freedom*

216 CALIS is capable of deploying sources at various positions inside LSV.  
 217 Besides movement along Z up to maximum cable length, it is possible to  
 218 articulate at an angle of  $\theta$  between  $0^\circ$  and  $90^\circ$ , where  $\theta$  is the zenith-angle  
 219 (Fig. 7). Angles of more than  $90^\circ$  are excluded because articulation chain's  
 220 end is reached at a  $90^\circ$  angle (see Fig. 4).

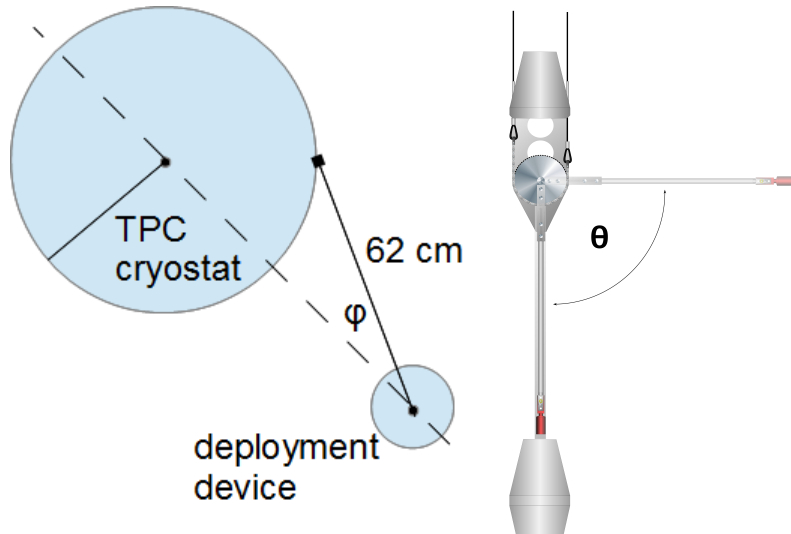


Figure 7: Two degrees of freedom in source deployment position after a certain source arm length has been chosen: *left*: rotation in XY-plane, *right*: articulation to an angle  $\theta$  between  $90^\circ$  when arm is articulated, and at  $0^\circ$  when dearticulated.

221 *2.7.1. XY-plane rotation*

222 A sealed connection below view port has an o-ring seal and uses a  
 223 ring clamp to compress seal. This clamp can be slightly loosened allowing  
 224 upper assembly (above and including view port) to be rotated with  
 225 respect to lower assembly and detector. Rotation in XY-plane can even be  
 226 performed while device is deployed next to cryostat, since seal is helium  
 227 leak and light tight even when loosened.

228 In principle a rotation in  $360^\circ$  can be done, except when arm would  
229 interfere with cryostat. This has been used in one calibration campaign  
230 to deploy a neutron source directly next to the cryostat and rotated away  
231 by  $90^\circ$  to study optical shadowing effects from cryostat (Sec. 4).

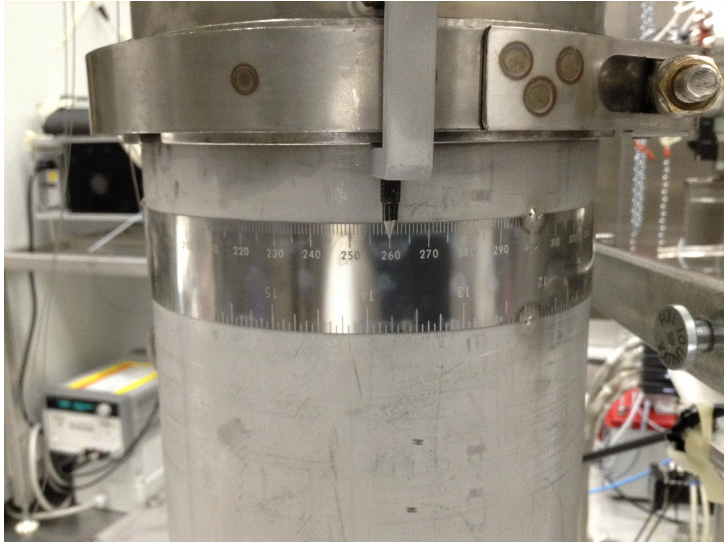


Figure 8: Beneath view port is a ring clamp with angle measuring strip underneath. To perform azimuthal rotation, ring clamp is slightly loosened, and entire upper assembly is rotated with respect to lower assembly, along with deployment device. Rotation angle is read from strip going around the pipe. Strip is in mm, which has then been calibrated in degrees.

232 2.7.2. “No fly” zone

233 A “no fly” zone is defined right above the cryostat where there are  
234 many TPC supply tubes. No deployment device part may enter in this  
235 region, in particular not the source arm.

236 2.7.3. Default configuration

237 By default, deployment device has been deployed with its longest arm  
238 (62 cm), at center of TPC’s active volume in vertical direction, with arm  
239 rotated in XY-plane until contact is made with cryostat.

240 Other degrees of freedom could involve shorter arm lengths, while  
241 longer arm lengths would require deployment device hardware modifi-  
242 cations. Out of four organ pipes a second one is available for source

243 calibration. (Two organ pipes are not available due to interference with  
244 existing infrastructure: the cryogenic tower and electronic rack.) Moving  
245 CALIS to a different organ pipe requires a more substantial effort involv-  
246 ing a partial CALIS disassembly and reinstallation on other organ pipe's  
247 gate valve.

### 248 **3. Testing, Cleaning and Commissioning**

249 CALIS has been assembled at FNAL from components produced at  
250 FNAL and University of Hawaii. After initial basic functionality tests  
251 at FNAL, CALIS was shipped pre-assembled to LNGS, where it under-  
252 went a comprehensive testing and calibration program. While still out-  
253 side clean room CRH, CALIS was installed on a high bay platform in the  
254 LNGS underground hall C and tested at its full length. Besides testing  
255 basic Z-motion, articulation and XY-rotation, all details of CALIS opera-  
256 tions ranging from testing functionality of motor controls, high limit and  
257 articulation switch to recovery scenarios after e.g. power failures during  
258 deployment were validated.

259 An important aspect was source's Z-position calibration as a function  
260 of cable length before and after source arm articulation, which is a nonlin-  
261 ear function of motor step counts, as mentioned in Sec. 2.2. Furthermore  
262 source's XY- and Z-position accuracy and precision was estimated.

263 This testing campaign's results were reviewed by an internal review  
264 board and approval for installation inside CRH was granted. CALIS was  
265 cleaned according to official cleaning procedures and installed on gate  
266 valve in September 2014. After installation on gate valve a testing focus  
267 was system's light and helium leak tightness, and nitrogen and vacuum  
268 systems testing, as these could only be tested fully after installation. A  
269 more detailed description of tests performed at FNAL and LNGS can be  
270 found in [6, 7].

#### 271 *XY- and Z-position*

272 Tests in air and in LSV's scintillator revealed source position accuracy  
273 and precision is dominated by uncertainties during articulation. Posi-  
274 tioning in Z before articulation is highly accurate and precise: deploy-  
275 ment speed is very low, barely visible to the naked eye (4 mm/s), which  
276 minimizes lateral motion during deployment and contact with housing  
277 or organ pipe is avoided during deployment. Yet during articulation a

swing in XY arises from tiny laterally imbalanced forces originating in articulating cable pull.

To ensure deployment precision a procedure has been worked out to make reliably gentle contact with the cryostat, thereby eliminating precision uncertainty in XY: After positioning deployment device in Z, source arm is articulated to horizontal while it is pointing away from the cryostat. Only then source is brought into contact with cryostat through a XY-rotation while monitoring photomultiplier tube (PMT) scaler rates, which increase while source is approaching, yet plateaus as soon as contact with the cryostat is made, even if XY-rotation continues. This provides a reliable XY- and Z-position for calibration source and was used throughout calibration campaigns.

## 4. Calibration Campaigns

### 4.1. Radioactive Sources

For calibration of LSV detector response and TPC's response to electron recoils (ER)  $^{57}\text{Co}$ ,  $^{133}\text{Ba}$  and  $^{137}\text{Cs}$  were selected.  $^{22}\text{Na}$  was deployed in a later calibration campaign. They allow a cross-calibration with  $^{83m}\text{Kr}$  injected in Argon recirculation system during dedicated campaigns and internal  $^{39}\text{Ar}$ , as they cover the  $^{39}\text{Ar}$  energy range (see also Table 1 and Fig. 9).

After a gamma source energies preselection, detailed studies with DarkSide Monte Carlo simulation package G4DS [8] were performed to select appropriate source activities and check various deployment positions' feasibility and physics reach. Sources with suitable activities were identified for deployment considering also constraints from LSV and TPC DAQs (Table 1).

Energy variables are calibrated in photo-electrons (PE) using dedicated laser calibration runs, in which each PMT's single PE charge spectra are fitted and a PE-charge gain is determined. These laser runs are also an integral part of a calibration campaign requiring a laser run every few hours and at least on each change in DAQ, TPC or CALIS configuration, such as drift field changes or source position changes.

### 4.2. Calibration Campaigns Timeline and Stability

Following calibration campaigns were performed between October 2014 and April 2016:

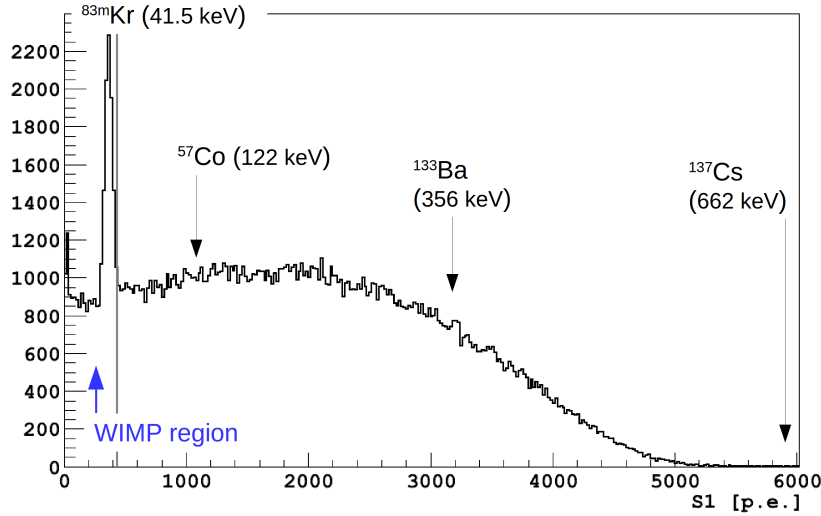


Figure 9: Scintillation spectrum (S1) at null field showing a  $^{83m}\text{Kr}$  peak on internal  $^{39}\text{Ar}$   $\beta$  spectrum. Positions of full absorption peaks of three gamma sources are indicated and cover  $^{39}\text{Ar}$  spectrum's full range.

Table 1: Gamma sources deployed in DS-50,  $^{39}\text{Ar}$  and  $^{83m}\text{Kr}$  [9].  $^{39}\text{Ar}$  activity has been approx. 50 Bq (1 Bq/kg) during AAr filling and negligible in the UAr phase. The Kr source activity varied from campaign to campaign, but was in range of a few Bq to some tens of Bq.

<b>source</b>	<b>type</b>	<b>energy</b>	<b>half life</b>	<b>activity</b>
$^{57}\text{Co}$	$\gamma$	122 keV	0.744 y	35 kBq
$^{133}\text{Ba}$	$\gamma$	356 keV	10.54 y	2 kBq
$^{137}\text{Cs}$	$\gamma$	662 keV	30.2 y	0.65 kBq
$^{22}\text{Na}$	$\gamma$	$2 \cdot 511 \text{ keV} + 1274 \text{ keV}$	2.603 y	11 kBq
$^{39}\text{Ar}$	$\beta$	565 keV endpoint	269 y	50 Bq
$^{83m}\text{Kr}$	$2\beta$	32.1 keV + 9.4 keV	86.2 d	varying

- 313 • First extensive campaign involving all gamma sources and both  
 314 high and low activity AmBe neutron source took place in October  
 315 and November 2014 at LNGS. TPC was filled with Atmospheric Ar-  
 316 gon with an inherent trigger rate of approx. 50 Hz from  $^{39}\text{Ar}$ . LSV  
 317 liquid scintillator consisted of PC only with < 0.1% TMB and 1.4  
 318 g/l PPO as wavelength shifter.
- 319 • In January and February 2015 a second campaign focusing on LSV  
 320 calibration using low activity AmBe source was performed. Be-  
 321 fore this LSV was reconstituted with 5% TMB. Two deployments  
 322 were performed at two different PPO concentrations (0.7 g/l and  
 323 1.4 g/l), allowing to study PPO concentration impact on alpha and  
 324 gamma quenching. (1.4 g/l is our nominal PPO concentration, see  
 325 also Fig. 13, right)
- 326 • In August 2015 a  $^{22}\text{Na}$  source was deployed next to cryostat for TPC  
 327 calibration. This was first gamma source calibration campaign after  
 328 UAr deployment within DarkSide-50.
- 329 • In December 2015 an  $^{241}\text{Am}^{13}\text{C}$  neutron source has been deployed,  
 330 allowing an in-depth study of detection efficiency of prompt neu-  
 331 tron recoil signal in absence of correlated 4.4 MeV gamma, obfusc-  
 332 ating neutron recoil signal in case of an AmBe source.

333 In dedicated analyses it has been shown that calibration campaigns  
 334 have not affected negatively light yield or introduced radioactivity into  
 335 the LSV [3].

### 336 4.3. TPC Calibration

337 A few calibration results are shown illustrating acquired calibration  
 338 data quality and their description in G4DS.

#### 339 4.3.1. $^{57}\text{Co}$ S1 energy

340 Fig. 10 shows a data-MC comparison of scintillation signal S1 spec-  
 341 trum of a  $^{57}\text{Co}$  calibration source deployed next to cryostat and close to  
 342 TPC active volume center. S1 distribution is overlayed by an equivalent  
 343 selection of G4DS MC simulation events.

The plot is  
from Paolo's  
G4DS  
talk  
DS2016,  
UCLA.  
Ideally one  
could get an  
official copy  
from the MC  
paper.

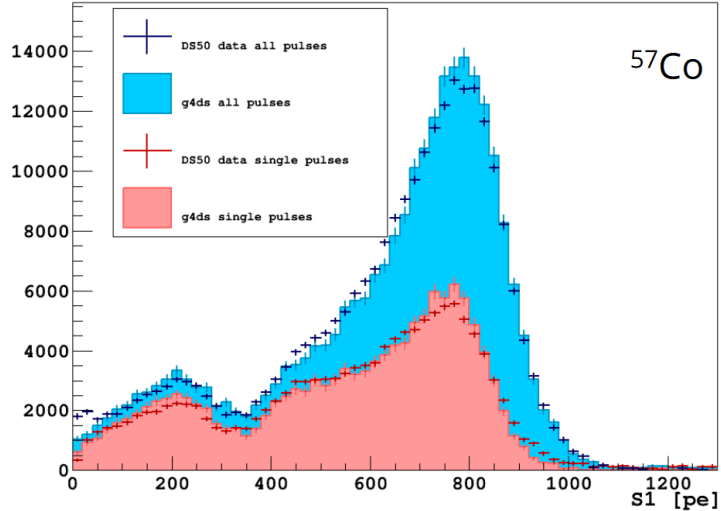


Figure 10: Data-MC comparison for  $^{57}\text{Co}$  source deployed next to cryostat. In magenta distribution a single-site interaction requirement is imposed as for dark matter events and for blue distribution this constraint is removed [8].

#### 344 4.3.2. F90 distribution from $^{241}\text{Am}^9\text{Be}$ neutron data

345 Fig. 11 shows good agreement between F90 medians and S1 spectra  
 346 measured from  $^{241}\text{Am}^9\text{Be}$  neutron data and those derived from SCENE  
 347 measurements, which have been used to determine nuclear recoil energy  
 348 scale and NR acceptance regions for WIMP dark matter search [1, 2].

#### 349 4.3.3. Source position

350 Tests at LNGS established the deployment system's positioning ac-  
 351 curacy to be about  $\pm 1$  cm after a 7 meter journey into the DarkSide-50  
 352 LSV. During first calibration campaign several runs have been taken with  
 353 source at its central position (731000 motor step counts). Fitting  $t_{drift}$   
 354 distribution at that position for a sequence of runs a systematic shift vs. time  
 355 has been observed (Fig. 12, right). The source position has been on aver-  
 356 age 157.4 mm below the grid with an RMS of 10.1 mm. Following that  
 357 observed systematic shift with time deployment procedures were revised  
 358 to avoid such a time dependency in the future and to improve the deploy-  
 359 ment precision: Prior to moving source to its target position, deployment  
 360 device is sent to its lowest position, where cables are fully unwound and  
 361 any build-up in the cables is released. It is worth mentioning this does  
 362 not induce significant uncertainties for calibration data analyses, as  $t_{drift}$   
 363 distribution can be measured in-situ on a per-run basis and hence does

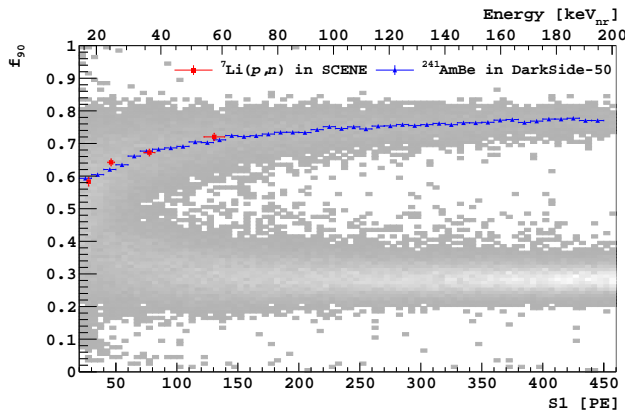


Figure 11: Plot of  $F_{90}$  vs. scintillation signal  $S_1$  from a high rate AmBe neutron source calibration of DarkSide-50 in grey, upper NR band from AmBe calibration and lower ER band from  $\beta$ - $\gamma$  backgrounds are visible. Overlaid are  $f_{90}$  NR median vs.  $S_1$  from a high-rate *in situ* AmBe calibration (blue) and scaled from SCENE measurements (red points) [10]. There is very good agreement between the two. High source intensity and correlated neutrons and  $\gamma$ -ray emission by AmBe source contribute events outside nuclear recoil and electron recoil bands. (reproduced from [2])

364 not affect our dark matter analysis.

365 For XY-position azimuthal angle distribution in XY-plane has been  
 366 studied and a 139 degree mean was observed with a 1.2 deg RMS. (One  
 367 degree corresponds to 6 mm at the outer cryostat, where source is po-  
 368 sitioned.) However an independent XY reconstruction algorithm gave  
 369 142.5 degrees with an 0.8 deg RMS, so that systematic uncertainties from  
 370 reconstruction dominate over XY precision.

#### 371 4.4. Liquid Scintillator Veto

372 In Fig. 13 (left) a data-MC comparison of LSV charge spectra from a  
 373  $^{137}\text{Cs}$  source deployed in LSV next to cryostat is shown [8]. In January  
 374 and February 2015 LSV scintillator reconstitution was completed and a  
 375 second LSV calibration using AmBe neutron source was undertaken to  
 376 further study various LSV neutron detection channels. With a borated  
 377 scintillator, a critical aspect of neutron detection efficiency is the capability  
 378 to observe 6.4 % capture branch leading to a 1775 keV  $\alpha + ^7\text{Li}(\text{g.s.})$  without  
 379 accompanying 478 keV  $\gamma$ -ray. As shown in Fig. 13 (right) the de-excitation  
 380 channel is clearly observed at around 30 PE.

*This is from DocDB 1288. Ideally one could cite a XY paper here, which is not published yet.*

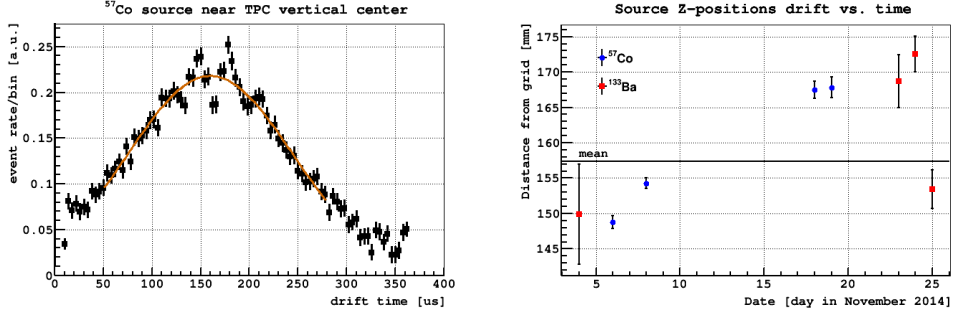


Figure 12: *left:* A  $t_{drift}$  distribution encoding the Z-position of a  $^{57}\text{Co}$  source deployed next to TPC vertical center. Single scatter events have been selected and background has been statistically subtracted. Fluctuations in otherwise smooth  $t_{drift}$  distribution are from Copper field cage rings surrounding the TPC. *right:* Shift of source position relative to TPC grid as a function of time when deployed to same place.

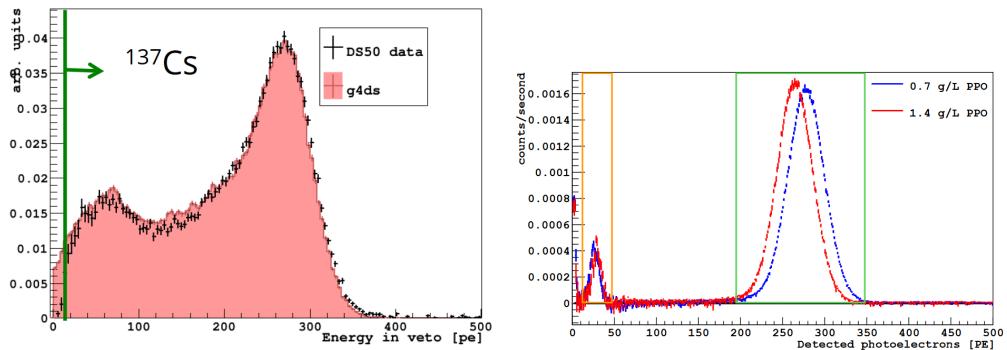


Figure 13: *left:* LSV charge spectra data-MC comparison from  $^{137}\text{Cs}$  source deployed in LSV next to the cryostat [8]. *right:* Clear neutron capture signal detection on  $^{10}\text{B}$  in LSV leading to a 1775 keV  $\alpha + ^7\text{Li}(\text{g.s.})$  at  $\approx 30$  PE (orange box). Peak on the right at  $\approx 270$  PE (green box) is from 93.6 % of captures that lead to the  $^7\text{Li}$  excited state reaction, with the accompanying 478 keV-ray. The entries below 10 PE are due to PMT after-pulses. Data has been taken before and after varying PPO wavelength shifter concentration in the scintillator with the source rotated 70 cm away from the cryostat. In both cases the deexcitation to ground state is clearly observed.[3]

381    **5. Conclusions**

382    CALIS is a simple and affordable, yet effective source deployment  
383    system that has been successfully used to deploy sources in LSV and  
384    next to TPC and to conduct several successful calibration campaigns. No  
385    adverse effects on the LSV or TPC have been noticed.

386    **6. Acknowledgements**

387    The DarkSide-50 Collaboration would like to thank LNGS laboratory  
388    and its staff for invaluable technical and logistical support. This report is  
389    based upon work supported by the US NSF (Grants PHY-0919363, PHY-  
390    1004072, PHY-1004054, PHY-1242585, PHY-1314483, PHY-1314507 and as-  
391    sociated collaborative grants; grants PHY-1211308 and PHY-1455351), the  
392    Italian Istituto Nazionale di Fisica Nucleare (INFN), the US DOE (Con-  
393    tract Nos. DE-FG02-91ER40671 and DE-AC02-07CH11359), and the Pol-  
394    ish NCN (Grant UMO-2012/05/E/ST2/02333). We thank the staff of  
395    the Fermilab Particle Physics, Scientific and Core Computing Divisions  
396    for their support. We acknowledge the financial support from the Uni-  
397    vEarthS Labex program of Sorbonne Paris Cité (ANR-10-LABX-0023 and  
398    ANR-11-IDEX-0005-02) and from the São Paulo Research Foundation (FAPESP).

This is a  
verbatim  
copy from the  
veto paper -  
adjustments  
needed?

399

- 400    [1] P. Agnes, et al., *First results from the DarkSide-50 dark matter experiment*  
401    *at Laboratori Nazionali del Gran Sasso*, [Phys. Lett. B, 743, 456](#) (2015).
- 402    [2] P. Agnes, et al., *Low radioactivity argon dark matter search re-*  
403    *sults from the {DarkSide}-50 experiment*, [arXiv:1510.00702 \[astro-ph,](#)  
404    [physics:hep-ex, physics:physics\]](#), (2015).
- 405    [3] P. Agnes and Others, *The veto system of the DarkSide-50 experiment*,  
406    [JINST, 11, P03016](#) (2016).
- 407    [4] T. I. Banks and Others, *A compact ultra-clean system for deploying ra-*  
408    *dioactive sources inside the KamLAND detector*, [Nucl. Instrum. Meth.,](#)  
409    [A769, 88](#) (2015).
- 410    [5] H. X. Huang and Others, *Manual Calibration System for Daya Bay Re-*  
411    *actor Neutrino Experiment*, [JINST, 8, P09013](#) (2013).

- <sup>412</sup> [6] B. Hackett, [*thesis title*].
- <sup>413</sup> [7] E. Edkins, [*thesis title*].
- <sup>414</sup> [8] P. Agnes, *The DarkSide-50 Monte Carlo simulation* To be published.
- <sup>415</sup> [9] W. H. Lippincott, et al., *Calibration of liquid argon and neon detectors with 83Krm*, [Phys. Rev. C, 81, 45803 \(2010\)](#).
- <sup>417</sup> [10] H. Cao, et al., *Measurement of scintillation and ionization yield and scintillation pulse shape from nuclear recoils in liquid argon*, [Phys. Rev. D, 91, 92007 \(2015\)](#).